

Parametric analysis of the seismic response of coupled tunnel–soil–aboveground building systems by numerical modelling

Glenda Abate¹ · Maria Rossella Massimino¹

Received: 18 July 2016 / Accepted: 21 July 2016 / Published online: 28 July 2016
© Springer Science+Business Media Dordrecht 2016

Abstract During an earthquake, the presence of tunnels may affect the seismic wave propagation in the involving soil and in turns the response of aboveground structures. At the same time, the vibrations of aboveground structures may create a complex interaction with the tunnel and, consequently, they may modify the dynamic response of the tunnel. Most of the published papers considered only tunnel–soil systems or only soil–aboveground structures; analyses involving tunnel plus soil plus aboveground structures (full-coupled analyses) are still very rare. The present paper deals with a parametric analysis: starting from a real case-history regarding the Catania (Italy) underground network, and in particular a cross-section including an aboveground building, the depth of the tunnel, the position of the aboveground building and the seismic inputs were modified in order to study their effects on the dynamic tunnel–soil–aboveground building interaction. Thirty different recorded accelerograms were adopted. Results are reported in terms of accelerations in the time and frequency domains, as well as in terms of seismic bending moments and axial forces of the tunnel lining.

Keywords Tunnel depth · Building distance · Equivalent-linear-visco-elastic constitutive models · Time and frequency domains · Accelerations · Seismic tunnel lining forces

List of symbols

a	Acceleration
D	Damping ratio
D_s	Soil damping ratio
D_l	Lining damping ratio

✉ Maria Rossella Massimino
mmassimi@dica.unict.it

Glenda Abate
glenda.abate@dica.unict.it

¹ Department of Civil Engineering and Architecture, University of Catania, Viale Andrea Doria 6, 95125 Catania, Italy

D_e	Epicenter distance
E_s	Soil Young elastic modulus
E_{s0}	Soil Young elastic modulus at small-strain
E_b	Building Young elastic modulus
E_l	Lining Young elastic modulus
F	Flexibility ratio
f_1	First fundamental frequency of the input
f_2	Second fundamental frequency of the input
f_m	Average fundamental frequency of the input
f_s	Natural frequency of the system
f_{1s}	First natural frequency of the system
f_{2s}	Second natural frequency of the system
f_{3s}	Third natural frequency of the system
G_s	Soil shear modulus
G_{s0}	Soil shear modulus at small strain
h	Tunnel depth
M	Dynamic bending moment
N	Dynamic axial force
R_a	Amplification ratio
$R_{a,av}$	Average value of amplification ratio
t	Time
T_b	Building predominant period
T_s	Soil predominant period
u_2	Horizontal axis
u_3	Vertical axis
V_s	Shear waves velocity
z	Vertical depth
α_r	First Rayleigh damping factor
β_r	Second Rayleigh damping factor
Δ	Distance of the building vertical axis from the tunnel vertical axis
γ_{max}	Maximum shear strain at tunnel depth
θ	Tunnel centre angle
θ_1	Rotation of the mesh nodes around the axis orthogonal to the investigated plane
ν_s	Soil Poisson ratio
ν_b	Building Poisson ratio
ν_l	Lining Poisson ratio
ω	Angular frequency

1 Introduction

Historically, underground structures have experienced a lower rate of damage than aboveground structures (Kawashima 2000). Nevertheless, recent studies have documented significant damage suffered by underground structures due to seismic events (Power et al. 1998; Hashash et al. 2001; Wang et al. 2001, 2009; Kontoe et al. 2008; Gazetas 2014). During an earthquake, the vibrations of aboveground structures may create a complex interaction with tunnels, and as a consequence they may affect the seismic wave propagation field (Lee and Karl 1992; De Barros and Luco 1993). Thus doing, they may modify

the dynamic response of tunnels while, at the same time, the presence of tunnels at shallow depth close to foundations of aboveground structures may alter the response of aboveground structures. Most of the published papers considered only tunnel–soil systems (St. John and Zahrah 1987; AFPS/AFTES, 2001; Hashash et al. 2005; Anastasopoulos et al. 2007, 2008; Anastasopoulos and Gazetas 2010; FHWA 2009; Lanzano et al. 2012), while a few considered tunnel–soil–aboveground structures (Luco and De Barros 1994; Kouretzis et al. 2007; Smerzini et al. 2009; Wang et al. 2013).

The present paper deals with a parametric analysis involving a full-coupled tunnel–soil–aboveground structure system. Starting from the underground network case-history of Catania (Italy) regarding a cross-section including an aboveground building (Abate and Massimino 2016), the depth of the tunnel, the position of the aboveground building and the seismic inputs were modified in order to study their effects on the dynamic tunnel–soil–aboveground building interaction. Thirty different recorded accelerograms were adopted.

Seismic waves impose different types of deformations on tunnels, such as: hoop compressions and extensions; longitudinal bending; ovaling or racking deformations. The component that has the most significant influence on the tunnel lining under seismic loading is the ovaling or racking deformations (Hashash et al. 2005; Pitilakis et al. 2014). For this reason, the present paper reports 2-D FEM analyses, which involve the transversal direction of the tunnel. Isotropic visco-elastic-linear behaviour was assumed for all the material involved; but, in order to take into account soil non linearity, the variations of the soil shear modulus and damping ratio with the strain–stress level, i.e. in turn with the input acceleration, were considered according to EC8 (2003).

Results are reported in terms of acceleration time-histories, amplification ratios, Fourier amplitude spectra and amplification functions. Bending moments and axial forces acting in the tunnel were also evaluated and compared with those obtained using the closed-form solutions proposed by Wang (1993) and Penzien (2000). The paper highlights the importance of complete full-coupled analyses, and in turns the influence of input frequency, tunnel depth, building position in the seismic response of tunnel–soil–aboveground structure systems.

2 The investigated tunnel–soil–aboveground building system

The investigated system regards the case-history presented in Abate and Massimino (2016). The main characteristics of this system are also reported in this paper for an easier reading of the present paper. A cross-section of Catania (Italy) underground is taken into account; it involves a full-coupled tunnel–soil–aboveground building system.

The tunnel is 11 m wide and 7.2 m high and it has a horseshoe section; its specific section is shown in Fig. 1. It is 18 m below the ground surface. It is a reinforced concrete structure, having conventionally a Young's modulus $E_1 = 28,500$ MPa, a Poisson's ratio $\nu_1 = 0.2$ and a damping ratio $D_1 = 5$ %.

The soil profile of the analysed section is characterised by the following stratigraphy (Fig. 1): anthropic layers ($RL + Ret$), silty clays (ALg) and clays (Aa). The sub-lithotypes ALg and Aa belong to the PSa lithotype. For this lithotype, the Young's modulus at very small-strain, E_{s0} , is equal to 300 MPa for the first 10 m, then it increases linearly from 300 to 1700 MPa. So, according to the Italian Technical Code NTC (2008), the soil can be classified as type C.

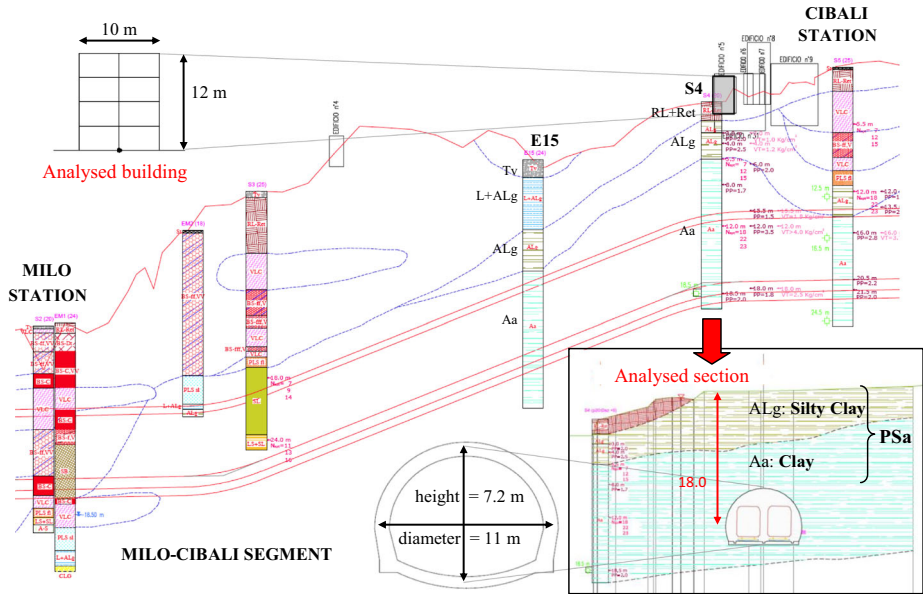


Fig. 1 The investigated tunnel–soil–aboveground building system

According to Merritt et al. (1985), the soil to tunnel relative flexibility is $F = 0.9$, considering an average radius of the horseshoe tunnel section; thus the tunnel is stiffer than the surrounding soil, i.e. the structural deformation level will be smaller than the free-field deformation level (rigid tunnel).

On the analysed section, there is a building, shown in Fig. 1. It is made of reinforced concrete ($E_b = 28,500 \text{ MPa}$, $\nu_b = 0.2$, $\gamma_b = 25 \text{ kN/m}^3$; $D_b = 5 \%$; conventional values); it is 10 m wide with two equal spans in the direction under investigation; it has four levels and the space between two levels is equal to 3 m. It has shallow foundations. The typical 2D frame of the building in the direction under investigation was taken into account in the FEM analysis. For the sake of simplicity, the building was assumed to rest on the soil surface.

The width of the considered soil deposit is fixed equal to 150 m in order to avoid as much as possible in the FEM modelling boundary effects on the tunnel and on the aboveground structure (see Sect. 3); the height of the soil deposit derives from geotechnical investigations according to which the bedrock is found at a depth of 38 m (Abate and Massimino 2016).

Actually two tunnel depths, h , were considered: the original one ($h = 18 \text{ m}$) and a second one ($h = 12 \text{ m}$). Similarly two distances, Δ , between the building vertical axis and the tunnel vertical axis were considered: the original one ($\Delta = 0 \text{ m}$) and a second one ($\Delta = 20 \text{ m}$). Thus four models were developed (Fig. 2). The first model (named Model 1) refers to the case-history discussed in Abate and Massimino (2016). The influence exerted by the depth of the tunnel and the position of the building was analysed separately. The assumed dimensions were not general enough to make a comprehensive parametric study; nevertheless, they allowed us some important considerations on full-coupled dynamic behaviour of tunnel–soil–aboveground structures to be developed.

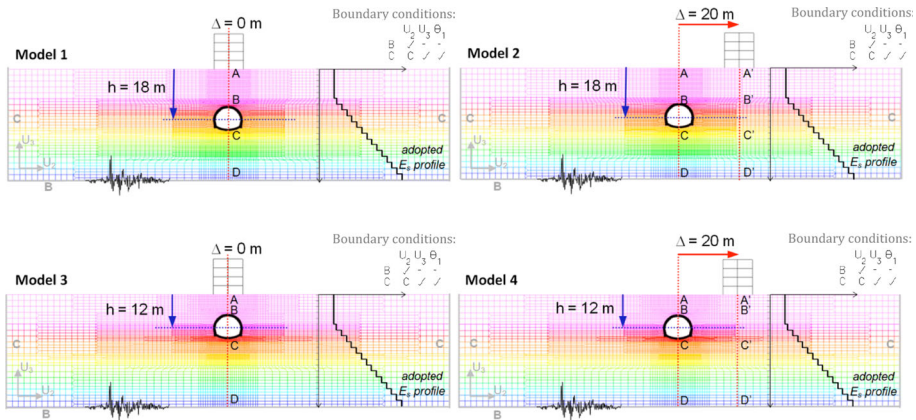


Fig. 2 The four adopted models, including boundary and seismic loading conditions, as well as Young modulus profile with depth (corresponding to different mesh colours) and the checkpoints A, B, C and D along the vertical tunnel axis and A', B', C' and D' along the vertical building axis, when the latter is 20 m far from the vertical tunnel axis

At the base of the developed four models thirty different accelerograms were adopted (Table 1; Fig. 3). All the accelerograms were in this case scaled to a $PHA = 0.1$ g. Generally, parametric studies actually do not refer to a “real” situation, thus the authors preferred to consider a low maximum input acceleration for which visco-elastic-linear constitutive model is more appropriated. The lower the PHA, the lower is the deformation level and, consequently, as the lower the strain level the more appropriate is the use of the visco-elastic-linear constitutive model. Afterwards, other ranges of acceleration could be investigated in comparison to that investigated in the case-history reported in Abate and Massimino (2016).

The average fundamental frequency f_m of all the inputs was evaluated by the Rathje et al. (1998) method. Then the inputs were subdivided in two groups: the first one characterised by a ratio $f_s/f_m \leq 0.4$; the second one characterised by a ratio $f_s/f_m > 0.4$, being f_s the natural frequency of the whole system. The first f_{1s} , the second f_{2s} and the third f_{3s} natural frequencies of the system were evaluated through a modal analysis performed by means of the ADINA code (Bathe 1996; ADINA 2008), taking into account the first three significant vibration modes for all the four FEM models in Fig. 2. In particular, Model 3 was characterised by the same natural frequencies as Model 1 ($f_{1s} = 0.83$ Hz, $f_{2s} = 1.26$ Hz, $f_{3s} = 2.20$ Hz), while Model 4 was characterised by the same natural frequencies as Model 2 ($f_{1s} = 0.83$ Hz, $f_{2s} = 1.55$ Hz, $f_{3s} = 2.26$ Hz). Thus, the building position was the only parameter, which influenced the modal analysis results.

Figure 4a and b show the ratios between the three natural frequencies of the system and the fundamental frequency of all the accelerograms for Models 1 and 3 ($\Delta = 0$ m) and Models 2 and 4 ($\Delta = 20$ m), respectively.

3 FEM modelling

The four full-coupled tunnel–soil–building systems described in Sect. 2 were analysed through the ADINA code (Bathe 1996; ADINA 2008), widely used in dynamic analyses (Grassi and Massimino 2009; Kirtas et al. 2009; Abate et al. 2006, 2015; Maugeri et al.

Table 1 Recorded accelerograms adopted as seismic inputs for the parametric analysis

Accelerograms	Name	Date (d/m/y)	De (km)	Recorded <i>PHA</i> (m/s^2)	Duration (s)	f_1 (Hz)	f_2 (Hz)	f_m (Hz)
E1	Valnerina, NS (Italy)	19/09/ 1979	5	2.01	24.97	1.35	4.50	3.17
E2	Lazio-Abruzzo, NS (Italy)	07/05/ 1984	68	1.29	22.87	2.16	4.70	6.48
E3	Etolia (Greece)	18/05/ 1988	23	1.62	30.43	2.90	2.10	2.75
E4	Oros Peninsula (Greece)	06/08/ 1983	76	1.07	17.65	3.82	4.20	4.17
E5	Umbria-Marche (Italy)	03/10/ 1997	27	2.78	24.25	7.80	3.10	3.79
E6	Sortino, EW (Italy)	13/12/ 1990	29	1.01	27.96	1.81	1.24	2.72
E7	Catania, NS (Italy)	13/12/ 1990	–	2.43	24.49	2.91	4.38	2.88
E8	Catania, EW (Italy)	13/12/ 1990	–	2.16	20.00	0.39	1.11	1.25
E9	Acireale (Italy)	20/02/ 1818	–	2.91	30.00	1.09	0.86	1.8
E10	Hyblaean (Italy)	13/12/ 1990	–	0.5	39.88	5.58	4.70	5.13
E11	Nebrodi, EW (Italy)	31/10/ 1967	–	2.42	49.86	4.18	2.72	3.41
E12	Ierissos (Greece)	26/08/ 1983	42	1.05	23.22	6.15	6.82	6.26
E13	Timfristos (Greece)	14/06/ 1986	9	3.02	10.38	12.70	6.86	7.45
E14	Timfristos (Greece)	14/06/ 1986	8	2.84	12.12	5.40	8.75	6.22
E15	Etolia (Greece)	18/05/ 1988	23	1.62	24.25	2.92	3.10	3.63
E16	Friuli (Italy)	06/05/ 1976	23	1.03	40.32	1.59	2.26	2.1
E17	Friuli (Italy)	07/05/ 1976	27	1.64	22.02	8.07	2.76	5.05
E18	Friuli, NS (Italy)	11/09/ 1976	8	1.59	29.40	5.53	4.54	4.11
E19	Friuli, NS (Italy)	15/09/ 1976	12	0.68	25.50	5.92	15.05	6.21
E20	Friuli, EW (Italy)	15/09/ 1976	12	1.03	25.50	5.25	3.47	4.64
E21	Friuli (Italy)	16/09/ 1977	9	1.84	44.94	2.64	4.93	4.14
E22	Valnerina, EW (Italy)	19/09/ 1979	5	2.07	49.86	7.01	8.14	7.8
E23	C. di Mazara (Italy)	07/06/ 1981	10	2.78	49.86	7.91	8.56	6.48

Table 1 continued

Accelerograms	Name	Date (d/m/y)	De (km)	Recorded PHA (m/s^2)	Duration (s)	f_1 (Hz)	f_2 (Hz)	f_m (Hz)
E24	Umbria (Italy)	29/04/1984	27	2.94	25.56	6.63	7.75	6.06
E25	Lazio-Abruzzo, EW (Italy)	07/05/1984	68	3.19	19.62	8.97	6.63	5.99
E26	Friuli, EW (Italy)	11/09/1976	8	1.83	29.40	2.95	3.68	2.98
E27	Arpiola (Italy)	22/03/1984	164	2.23	19.98	4.94	3.87	4.11
E28	Vrancea (Romania)	30/08/1986	49	1.41	16.44	1.49	2.78	1.95
E29	Spitak (Turkey)	01/11/1991	6	0.97	17.34	13.22	7.12	8.13
E30	Kozani (Greece)	13/05/1955	17	1.4	29.22	2.91	4.81	3.82

2012). Transient dynamic analyses were performed using the full-Newton iteration method and the Newmark implicit integration method. A number of steps ranging between 1039 and 7993 for a corresponding step magnitude ranging between 0.01 and 0.004 s were adopted according to the input acceleration time histories (Table 1).

For all the four investigated tunnel–soil–aboveground building models, Fig. 2 reports the mesh, the boundary and seismic loading conditions, the E_s profile and the checkpoints A, B, C, and D along the vertical axis of the tunnel and A', B', C' and D' along the axis of the buildings, when the latter is 20 m far from the vertical axis of the tunnel. The soil was modelled by 9-node solid rectangular elements and it was divided into 15 horizontal layers with different coloured soil layers according to the actual Young modulus profiles with depth discussed in Sect. 2 and more extensively in Abate and Massimino (2016). More precisely, moving from the soil surface, the first layer has a thickness of 10 m, then there are 14 layers, each of a thickness equal to 2 m.

A linear-equivalent-visco-elastic behaviour was used for the soil. To take into account soil non linearity, the Young's modulus at small strain E_{s0} was reduced in line with EC8 (2003) (Table 2). The Young's modulus at small strain E_{s0} was reduced in line with EC8 (2003) (Table 2). By considering that the PHA of input motions at the bedrock was fixed equal to 0.1 g (see Sect. 2) and that the expected PHA at the ground surface is approximately equal to $0.1 \times 1.4 = 0.14$ g (being 1.4 the estimated amplification ratio according to NTC, 2008) $E_s/E_{s0} = 0.80\%$ was fixed, being $E_s = G_s (1 + \nu_s)$ and $\nu_s = 0.3$. For the same reason, the soil damping ratio D_s was assumed equal to 3%.

The tunnel and the building were modelled by 2-node beam elements, adopting a linear visco-elastic constitutive model, considering the usual values of the reinforced concrete, reported in Sect. 2.

Similarly to what discussed in Abate and Massimino (2016), the mesh element minimum size was chosen in order to be 1/6/1/8 of the minimum wavelength, in order to ensure the efficient reproduction of all the waveforms of the whole frequency range under study. Moreover, a finer discretization near the tunnel and the building was selected in order to

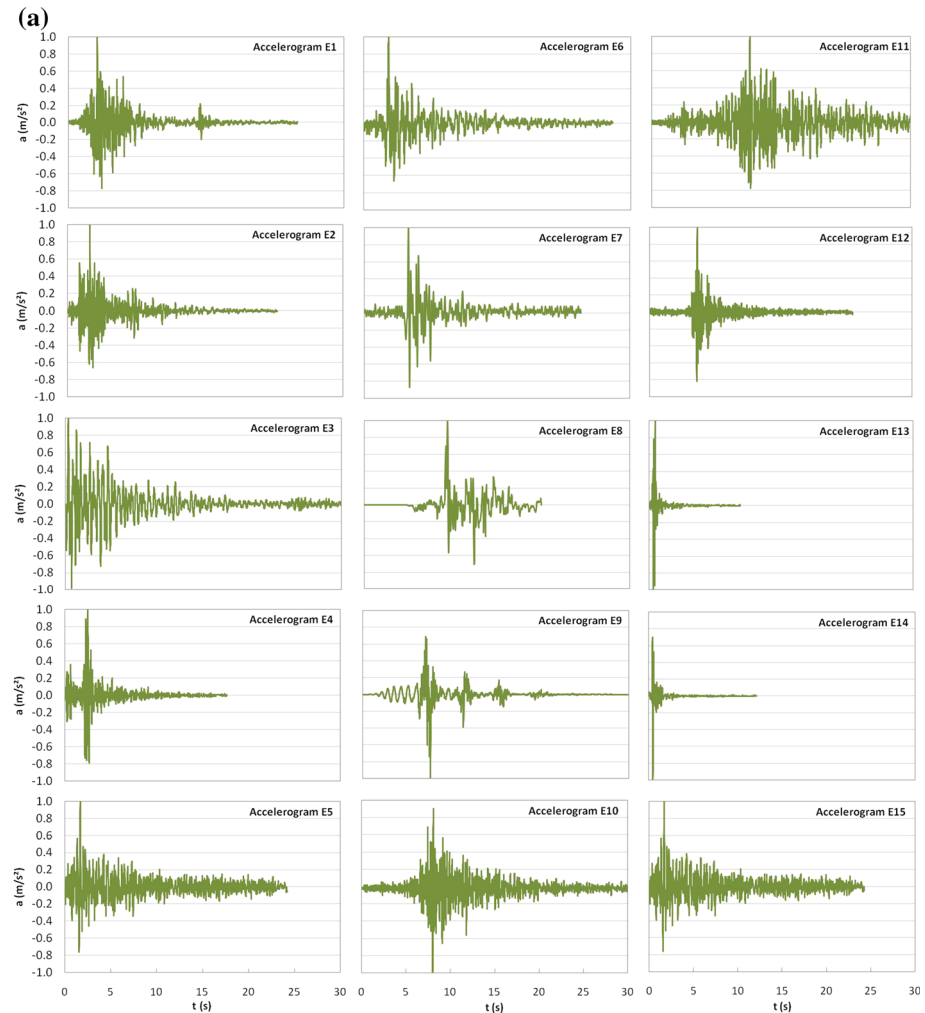


Fig. 3 Recorded accelerograms adopted as seismic inputs, scaled to $PHA = 0.1$ g: **a** Accelerograms from E1 to E15; **b** accelerograms from E16 to E30

ensure an efficient modelling of the soil close to the tunnel and to the building, as well as an efficient modelling of the tunnel and the building.

For the sake of simplicity, a solid connection between the soil and the tunnel was assumed, i.e. no slip conditions are supposed. Although interface characteristics are important for the dynamic response of embedded structures, this assumption is quite common in engineering practice (Huo et al. 2005; Sedarat et al. 2009; Tsinidis et al. 2013a, b; Pitilakis and Tsinidis 2014; Pitilakis et al. 2014).

In order to minimize as much as possible the reflection of waves into the domain in a very easy-to-use way, the nodes of the vertical boundaries were linked by “constraint equations” that impose the same horizontal translation at the same depth (Gajo and Muir Wood 1997; Abate et al. 2008, 2010). Moreover, the vertical boundaries of the soil deposit

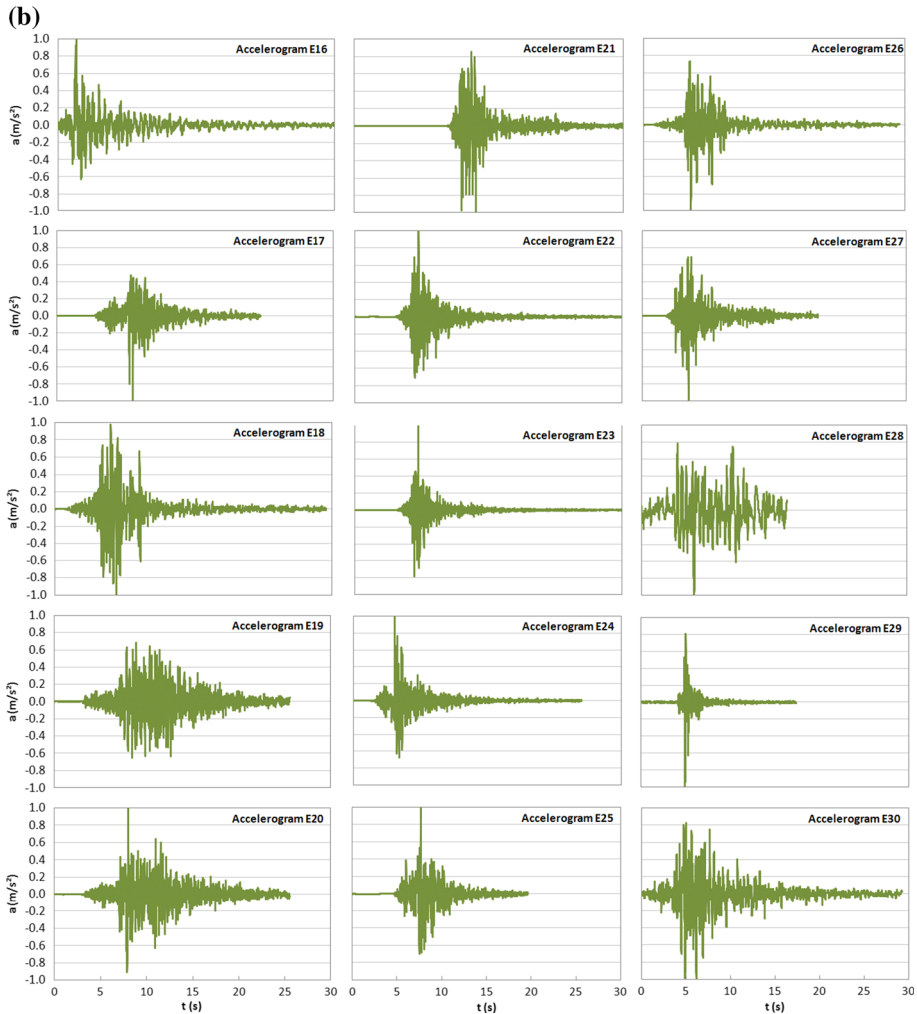


Fig. 3 continued

were located at a distance from the tunnel equal to about 6 times the tunnel width (total width of the soil deposit = 150 m). Finally, all the nodes of the base of the mesh were restrained in the vertical direction, because the bedrock was found at this depth (38 m) according to the geotechnical investigation discussed in Sect. 2.

The Rayleigh damping factors α_r and β_r were computed according to the well-known relations (Chang et al. 2000; Lanzo et Al. 2003): $\alpha_r = D \cdot \omega$ and $\beta_r = D/\omega$, being D the damping ratio and ω the angular frequency of the involved systems. More precisely, different values of α_r and β_r were computed for the tunnel ($\alpha_r = 0.735$; $\beta_r = 0.003$), the soil ($\alpha_r = 0.441$; $\beta_r = 0.002$) and the building ($\alpha_r = 0.650$; $\beta_r = 0.004$) according to the different values of D discussed previously. The angular frequency ω is evaluated according to first fundamental periods of the systems, being $\omega = 2\pi/T$. As discussed in Abate and Massimino (2016), the first fundamental period of the building was $T_b = 0.48$ s according to the Italian Technical code (NTC 2008) and the first fundamental period of the soil was

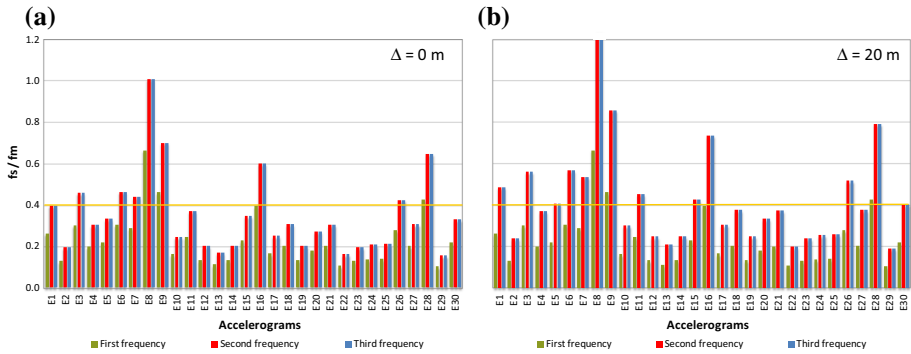


Fig. 4 Ratios between the natural frequency of the system (f_s) and the main frequency of the seismic input (f_m): **a** Models 1–3, **b** Models 2–4

Table 2 Average soil damping ratios and average reduction factors (\pm one standard deviation) for shear wave velocity V_s ($V_s/V_{s,max}$) and shear modulus G_s (G_s/G_{s0}) according to the peak horizontal acceleration at the soil surface (after EC8 2003)

Ground acceleration (g) $S_s \cdot PHA_{input}$	Damping ratio	$V_s/V_{s,max}$	G_s/G_{s0}
0.10	0.03	0.9 (± 0.07)	0.80 (± 0.10)
0.20	0.06	0.7 (± 0.15)	0.50 (± 0.20)
0.30	0.10	0.6 (± 0.15)	0.36 (± 0.20)

Through the \pm one standard deviation ranges, the designer can introduce different amounts of conservatism, depending on such factors as stiffness and layering of the soil profile. Values of $V_s/V_{s,max}$ and G_s/G_{s0} above the average could, for example, be used for stiffer profiles, and values of $V_s/V_{s,max}$ and G_s/G_{s0} below the average could be used for softer profiles

The bold values are the ones chosen for the numerical analyses

$T_s = 0.43 s$ according to Idriss and Seed (1968). The first fundamental period of the tunnel was assumed equal to that calculated for the soil, because the tunnel and the soil, being closely related, typically respond in agreement to the movement induced by the earthquake.

All the analyses were performed in two steps, the one next to the other: in the first step a static analysis was performed (static step) considering static vertical distributed loads and concentrated forces on the building, due to design surcharges; while in the second step the earthquake input motion was applied at the bottom of the model (dynamic step). Moreover, both for the static and for the dynamic steps a “mass proportional load” was applied to the whole system, in order to take into account the gravity loads. Thus, strain state obtained from the static step is accumulated for the dynamic step.

4 Results of the parametric analysis

4.1 Response in terms of accelerations in the whole system

The first phase of the parametric analysis consisted in studying the amplification or de-amplification phenomena, considering all the possible combinations: (1) $f_s/f_m \leq 0.4$ or $f_s/$

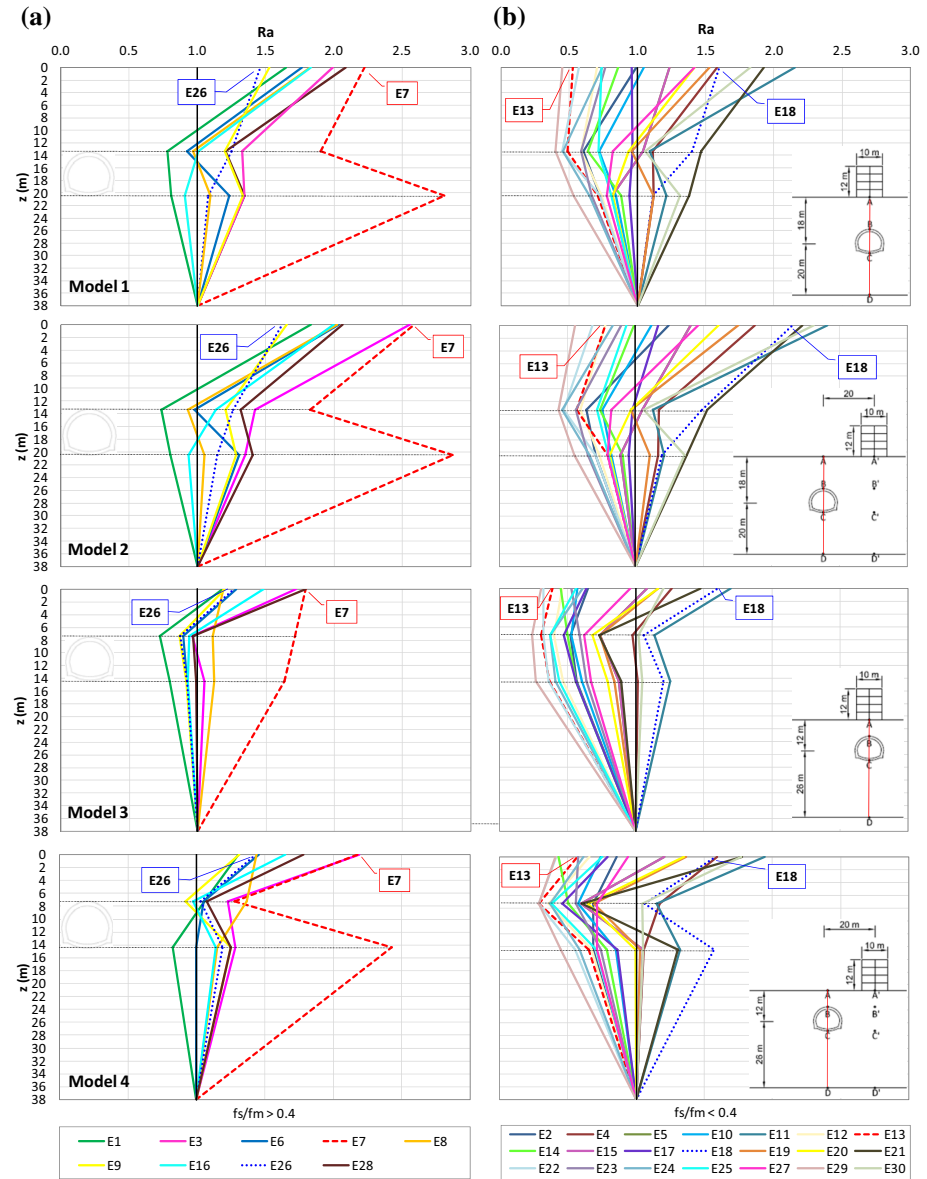


Fig. 5 Amplification ratios for the four models: **a** accelerograms for which $f_s/f_m \leq 0.4$; **b** accelerograms for which $f_s/f_m > 0.4$

$f_m > 0.4$; (2) shallow or deep tunnel; (3) building aligned to the vertical axis of the tunnel or unaligned with it.

Figures 5 and 6 show the seismic response in terms of amplification ratios, while Fig. 7 shows the seismic response in terms of Fourier amplitude spectra and amplification functions. Other results in terms of amplification ratio and maximum acceleration are reported in “Appendix”. Two different alignments were considered: the A–D alignment,

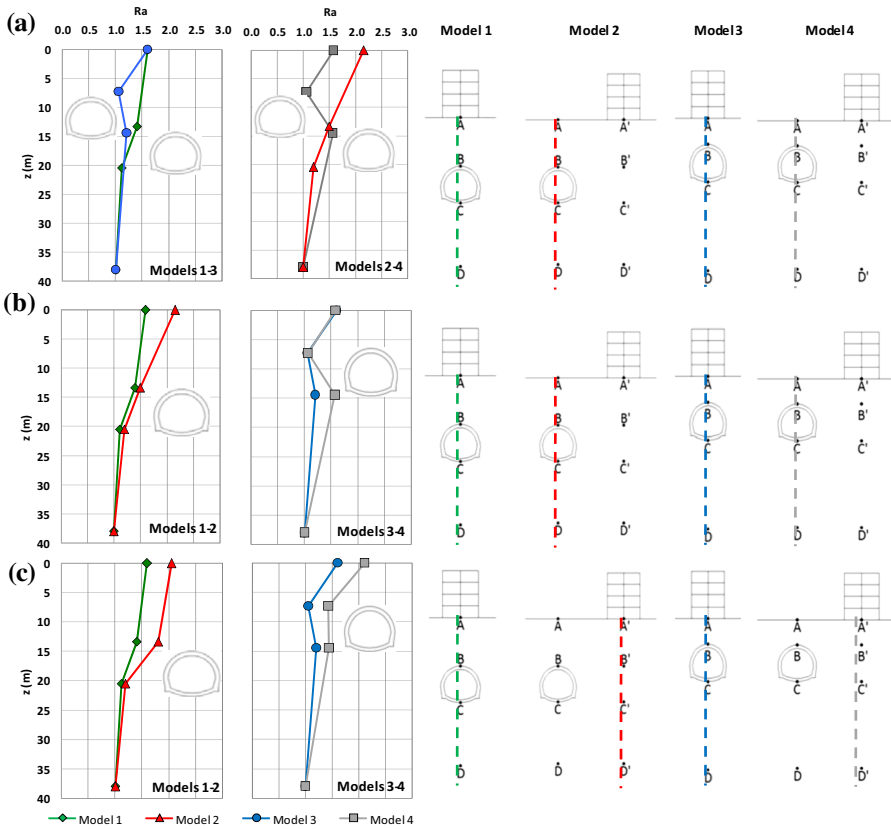


Fig. 6 Amplification ratios for the four models applying seismic input E18: **a** influence of the tunnel depth along the axis of the tunnel (A–D alignment); **b** influence of the building position along the axis of the tunnel (A–D alignment); **c** influence of the building position along the axes crossing the building (A–D and A’–D’ alignment)

along the axis of the tunnel and the aligned building, and the parallel A’–D’ alignment, along the axis of the unaligned building (considered for Models 2 and 4). It is obvious that the depth of the B and C nodes (and the corresponding B’ and C’ nodes) are different for Models 1–2 and 3–4.

Figure 5 shows the amplification ratio R_a for the four models analysed, considering the different effects of the inputs; in particular, Fig. 5a shows the R_a values related to the accelerograms for which $f_s/f_m > 0.4$; instead, Fig. 5b shows the R_a values related to the accelerograms for which $f_s/f_m \leq 0.4$. For the cases with a deep tunnel (Models 1 and 2), R_a at the soil surface is only slightly greater than 1.5 for the inputs characterised by $f_s/f_m > 0.4$; instead it is very often lower than 1.5 for the other inputs. For the cases with a shallow tunnel (Models 3 and 4), R_a at the soil surface is always greater than 1.0 for the inputs characterised by $f_s/f_m > 0.4$, instead it is sometimes lower than 1.0 and sometimes greater than 1.0 for the other inputs. Therefore, for the inputs characterised by $f_s/f_m > 0.4$ there is always an amplification of the seismic input ($R_a > 1$ at the soil surface), which was much more evident for those cases characterised by a deep tunnel. For the inputs

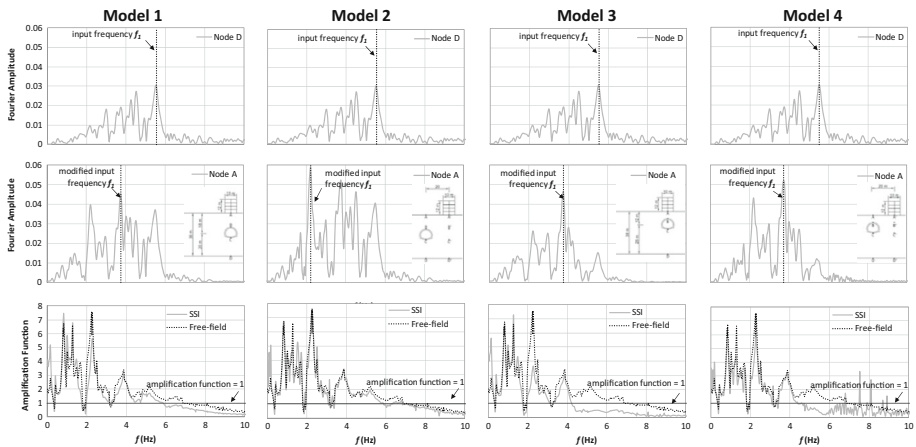


Fig. 7 Fourier spectra along the A–D alignment (first row for node D, second row for node A) and amplification functions (third row) in the soil for E18, considering the full-coupled tunnel–soil–aboveground structure system (continuous line, named SSI) and the free-field conditions (dashed line, named free-field)

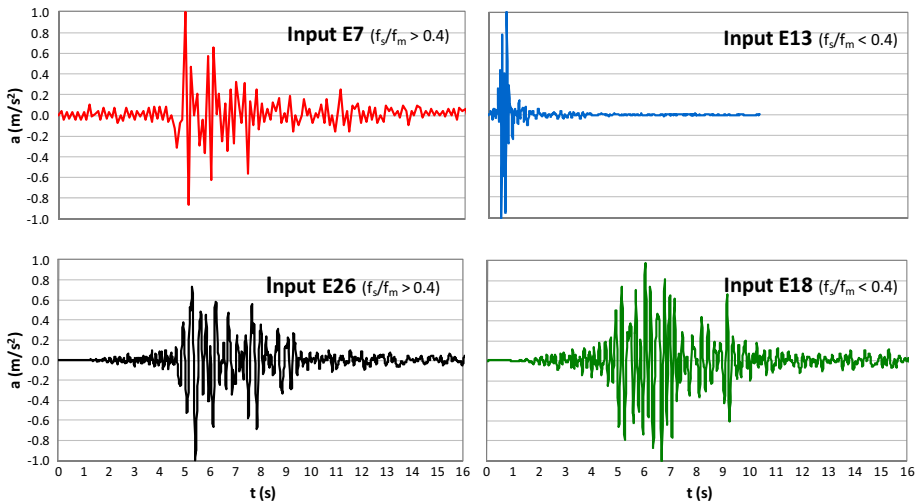


Fig. 8 Acceleration time-histories of the four inputs chosen for the analyses in terms of bending moments and axial forces along the tunnel

characterised by $f_s/f_m \leq 0.4$, a de-amplification of the seismic input ($R_a < 1$ at the soil surface) can occur, above all for those cases characterised by a shallow tunnel.

As regards the effect of the tunnel on the soil response, for the inputs characterised by $f_s/f_m > 0.4$ (Fig. 5a), generally both amplification and de-amplification are possible from the bedrock to the tunnel (from D to C). Then de-amplification of the input occurs across the tunnel (from C to B) above all for the cases characterised by a shallow tunnel. Finally, there is an amplification across the layer above the tunnel, which was stronger than the

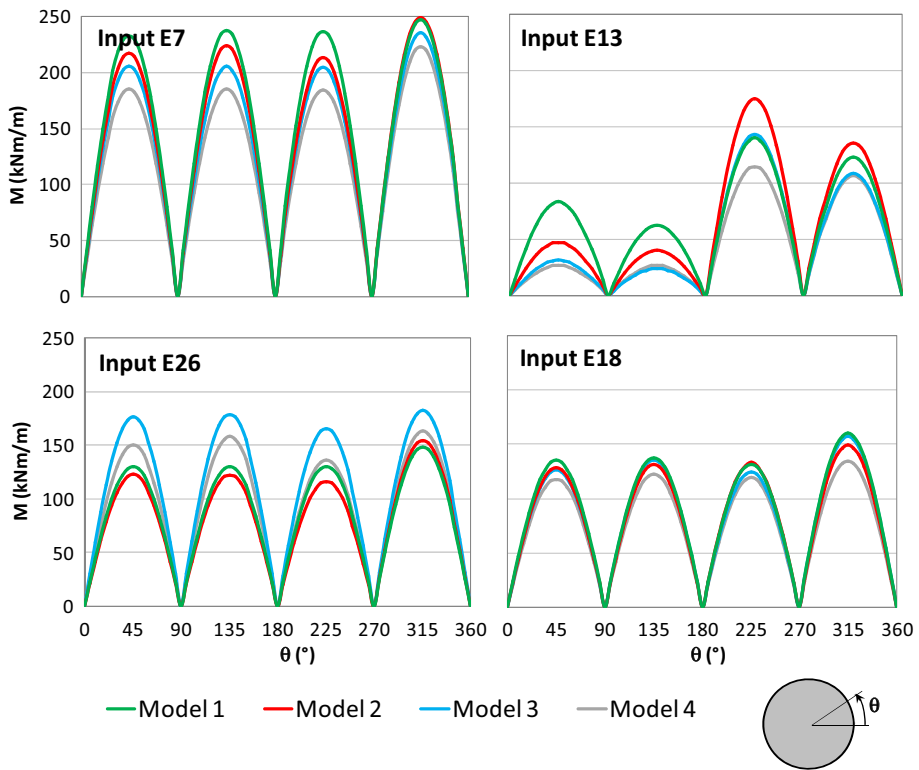


Fig. 9 Dynamic bending moment increments along the perimeter of the tunnel: influence of the position of the building and the depth of the tunnel, considering the four inputs chosen for the analyses

amplification of the input from the bedrock to the tunnel due to the E_s profile. This amplification at the soil surface is greater for the cases with a deep tunnel.

For the inputs characterised by $f_s/f_m \leq 0.4$ (Fig. 5b), there is generally a de-amplification of the input from D to C, followed by a further de-amplification across the tunnel (from C to B), which is much more significant in the cases with a shallow tunnel. Then, there is an amplification of the input across the layer above the tunnel (from B to A), which is more significant in the cases with a deep tunnel.

Therefore, as regards the effect of the depth of the tunnel, the amplification ratios in the cases of the shallow tunnel ($R_{a,av} = 1.05$ for $f_s/f_m \leq 0.4$ and $R_{a,av} = 1.55$ for $f_s/f_m > 0.4$; Models 1–2) are lower than the values achieved for the deep tunnel ($R_{a,av} = 1.30$ for $f_s/f_m \leq 0.4$ and $R_{a,av} = 1.88$ for $f_s/f_m > 0.4$; Models 3–4). The shallower soil layers being softer, the presence of the tunnel in these layers avoid the typical amplification in soft layers. The tunnel has a beneficial effect in terms of R_a , which become more evident as the tunnel depth become shallower.

As regards the effect of the position of the building in respect to the tunnel, the amplification ratios in the cases with an aligned building and tunnel (Models 1 and 3) are lower than the values achieved for an unaligned building (Models 2 and 4), because the building above the tunnel represented a surcharge, which reduced amplification phenomena. This effect disappears with depth and with the distance to the tunnel.

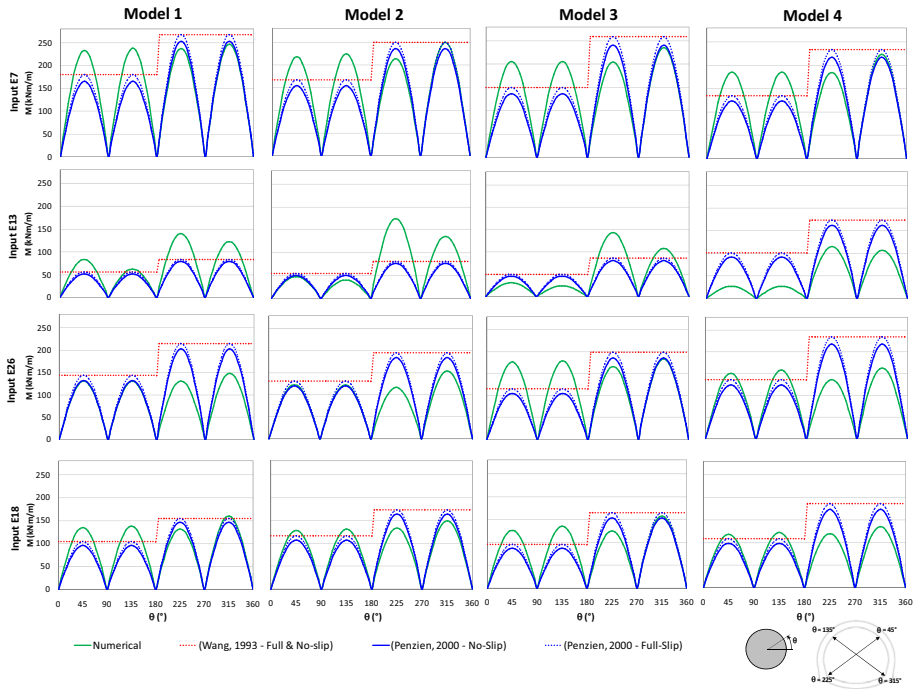


Fig. 10 Dynamic bending moment along the perimeter of the tunnel: comparison between numerical and analytical results (γ_{max} computed by FEM modelling of the complete soil–tunnel–aboveground building system with the ADINA code)

Figures 14, 15, 16, 17 (See “Appendix”) show once more the effects of tunnel depth, building position and input frequency on the seismic response of the system, giving similar results of Fig. 5.

Finally, the effects of the tunnel depth and the building position are shown in detail in Fig. 6 for seismic input E18; the latter was chosen from the accelerograms that gave $R_a > 1.5$ at the soil surface.

As regards the variation of the depth h of the tunnel, Fig. 6a reports the amplification ratios R_a along the axis of the tunnel (the A–D alignment), with the same position of the building. So, the comparison regards Model 1 versus Model 3 and Model 2 versus Model 4. As previously observed, the deeper the tunnel, the higher the amplification. When the tunnel is in the deepest position it reduces amplification phenomena in the stiffest soil layer.

Regarding the variation of the position Δ of the building with respect to the tunnel, the R_a values along the axis of the tunnel (A–D alignment) for Models 1 and 2 and Models 3 and 4 at equal tunnel depths, are compared in Fig. 6b. It is also possible to observe that the nearer the building to the tunnel, the lower the amplification. The presence of the building increased the mass and the stiffness along the investigated vertical axis of the tunnel, which in turn reduced amplification phenomena.

Finally, Fig. 6c regards the presence of the tunnel, reporting the amplification ratios R_a along the axes A–D and A’–D’ crossing the building. Comparing alignment A–D with alignment A’–D’ in this case, it is possible to investigate the effect of the presence of the

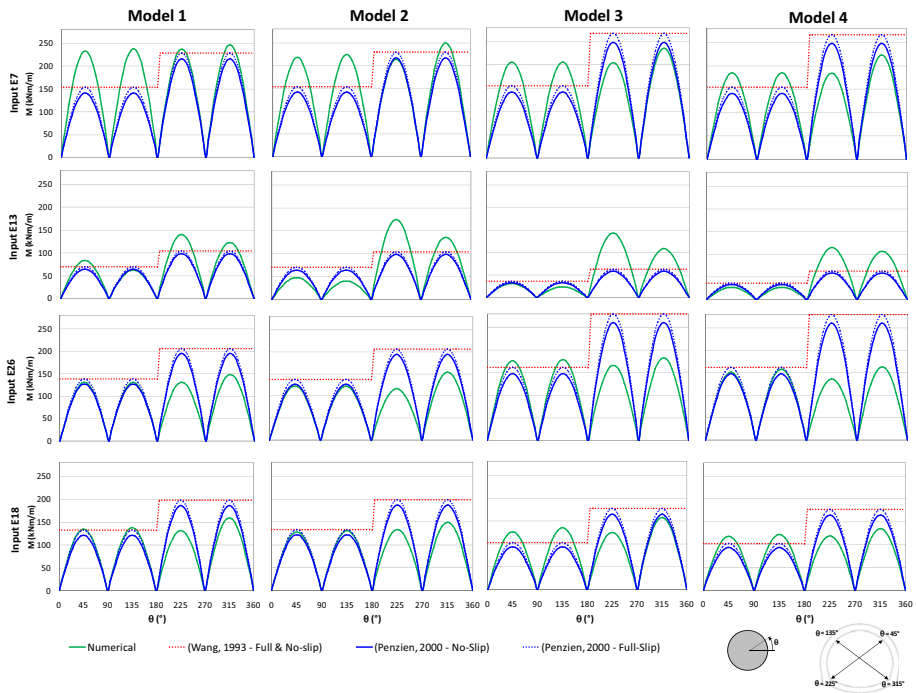


Fig. 11 Dynamic bending moment along the perimeter of the tunnel: comparison between numerical and analytical results (γ_{max} computed by 1D modelling for free-field conditions with the EERA code)

tunnel: the latter reduced the value of R_a at the soil surface regardless of the depth of the tunnel.

Moreover, with reference once more to the E18 input, Fig. 7 shows the Fourier amplitude spectra (*FASs*) along the A–D alignment for all the investigated models.

As expected the *FAS* at node D (i.e. at the base of the models, see first row) clearly shows the first fundamental frequency of the input (5.53 Hz); while the *FAS* of the acceleration time histories at node A shows different fundamental frequencies according to the filter effect of the system (see second row). Models 1, 3 and 4 cause a reduction of the input frequency up to 3.76 Hz and Model 2 causes a reduction of the input frequency up to 2.22 Hz. Free-field conditions cause a reduction of the input frequency up to 2.20 Hz. Model 2 along the A–D alignment is the nearest to the free-field condition at the soil surface. The results shown in Fig. 7 are very important, but they are very often neglected in the seismic design of new structures or retrofitting of old structures. The system under an aboveground structure always modifies the inputs that hit the aboveground structure, not only in terms of peak ground acceleration (see previous analysis in terms of R_a), but also in terms of fundamental frequency.

Figure 7 also shows the amplification functions (*AFs*), computed by normalizing the *FAS* at node A with respect to the *FAS* at node D (see third row). The *AF* for the free-field conditions are also added. The *AF* for the free-field conditions shows three significant peaks at the following frequencies: 0.83, 1.28 and 2.27 Hz. It is interesting to note that the frequency at which the highest peak is reached is 2.27 Hz. The above-mentioned frequencies give the most significant peak also for Models 2–4, but some interesting

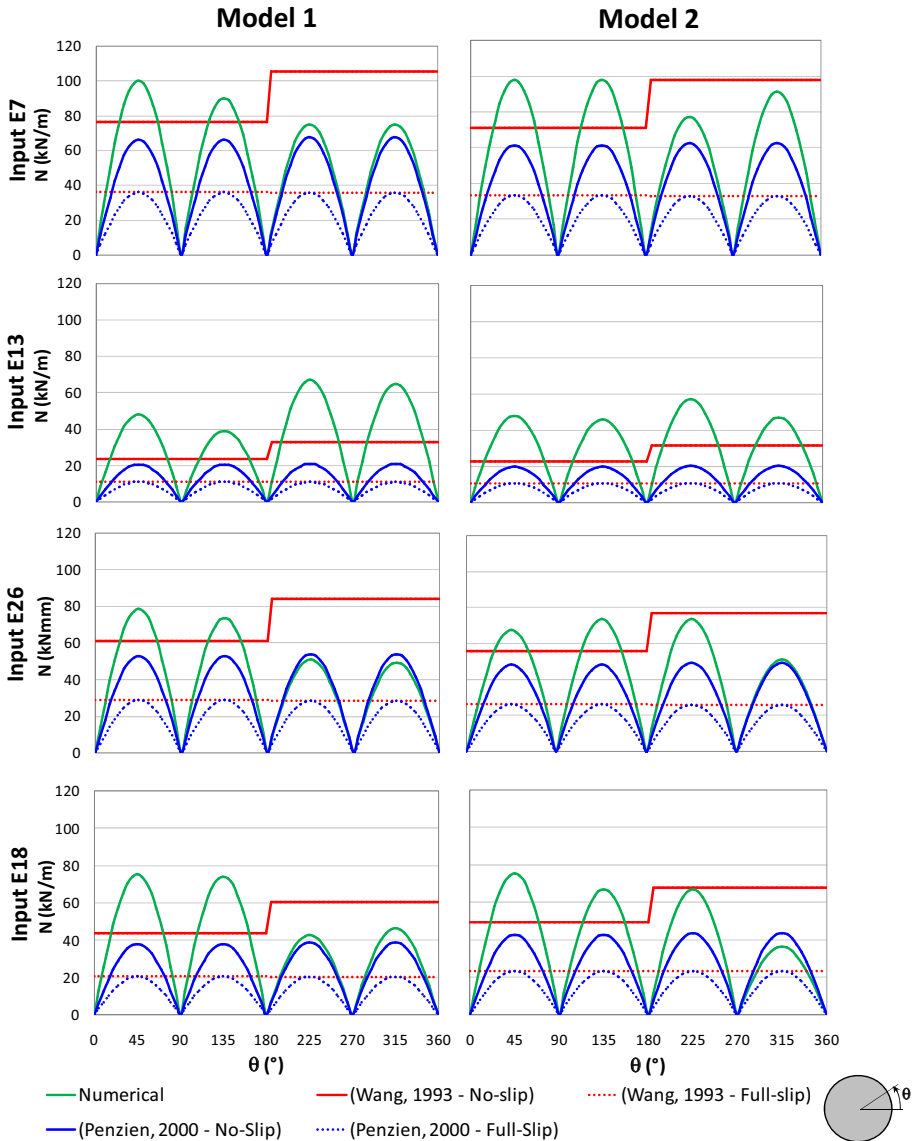


Fig. 12 Dynamic axial force along the perimeter of the tunnel: comparison between numerical and analytical results (γ_{max} computed by FEM modelling the complete soil–tunnel–aboveground building system with the ADINA code)

differences exist between the *AF* for the free-field conditions and the *AFs* of the four models. The second natural frequency for the free-field conditions (1.28 Hz) is not visible in Model 2 and Model 4. In particular, Model 2 shows a second critical frequency at 1.55 Hz. The most significant frequency in free-field conditions (2.27 Hz) is the least significant in Models 1 and 3. Comparing the *AF* of Model 1 with that of Model 2 and the free-field conditions, as well as comparing the *AF* of Model 3 with that of Model 4 and the

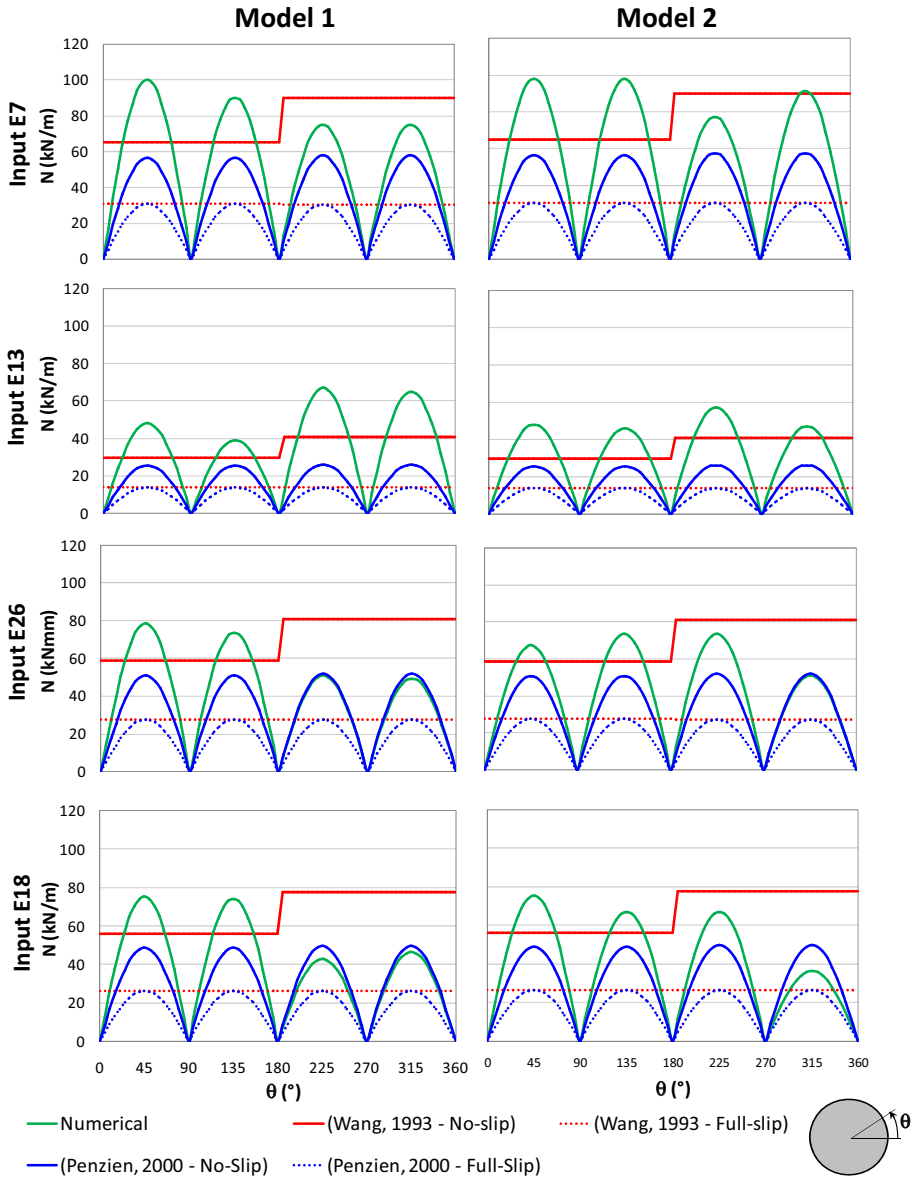


Fig. 13 Dynamic axial force along the perimeter of the tunnel: comparison between numerical and analytical results (γ_{max} computed by 1D modelling for free-field conditions with the EERA code)

free-field conditions, it is possible to observe that the presence of the aboveground building leads to a decrease in the most significant natural frequencies of the system; this is more evident when the tunnel is shallower. Comparing the AF of Model 1 with that of Model 3 and the AF of Model 2 with that of Model 4, it is possible to observe the effect of the depth of the tunnel: the shallower the tunnel, the lower the peaks; the natural frequencies do not change.

Thus, from Figs. 5, 6 and 7 it is globally possible to say that up to the maximum investigated tunnel depth (18 m) and the maximum investigated building distance (20 m) full-coupled consideration appear necessary.

4.2 Response in terms of tunnel bending moments and axial forces

The parametric analysis also investigated the response of the system in terms of bending moments and axial forces in the tunnel in the lining, in the transverse section per unit of longitudinal dimension. The numerical values, which correspond to the maximum values of the time-history responses, are taken into account. Due to the lack of space, only the four inputs reported in Fig. 8 were chosen for this aspect. According to Fig. 4, the E7 and E26 inputs are characterised by a ratio $f_s/f_m > 0.4$, instead the E13 and E18 inputs are among those characterised by a ratio $f_s/f_m \leq 0.4$. Moreover, as shown in Fig. 5, inputs E7 and E18 always lead to high amplifications, unlike inputs E13 and E26.

Figure 9 shows the dynamic bending moments for the two positions of the building and the two depths of the tunnel. On the basis of the information in Fig. 9 it is not possible to draw general conclusions about the effect of the tunnel depth on the tunnel bending moments. On the contrary, the position of the building has a clear effect: the nearer the building, the higher the dynamic bending moments.

Figures 10 and 11 show a comparison between the numerical bending moments and those estimated using the well-known analytical solutions proposed by Wang (1993) and Penzien (2000), which refer to the simpler tunnel–soil interaction (neglecting the above-ground building). These latest analytical solutions are discussed in Abate and Massimino (2016). In Fig. 10, the maxima shear strains, γ_{max} , used in the analytical solutions were computed by the FEM full-coupled soil–tunnel–aboveground building modelling. In Fig. 11 γ_{max} were computed for simple free-field conditions, i.e. ignoring the building and the tunnel, by 1D modelling performed using the EERA code (Bardet et al. 2000), employed for equivalent-linear earthquake site response analyses in free-field conditions.

Finally, Figs. 12 and 13 show a comparison between the numerical axial forces and those estimated using the analytical solutions proposed by Wang (1993) and Penzien (2000). Once again, in Fig. 12, the maxima shear strains, γ_{max} , used in the analytical solutions, were computed by the FEM full-coupled soil–tunnel–aboveground building modelling. In Fig. 13 γ_{max} were computed by the 1D modelling performed using the EERA code (Bardet et al. 2000) for simple free-field conditions.

Generally, it is possible to observe a quite good agreement between the numerical and analytical results. In particular, a remarkable agreement is achieved between the numerical and analytical results when computing γ_{max} with the full-coupled FEM modelling. Moreover, as discussed in Abate and Massimino (2016), the analytical solutions refer to a circular tunnel, while the tunnel investigated in the present paper has a “horseshoe tunnel section” and this difference contributes to the differences observed between the numerical and analytical results. Finally, in terms of bending moments the difference between full-slip and no-slip conditions is negligible, while it is evident in terms of axial forces. Analytical solutions for no-slip conditions are more conservative and nearer to the numerical results obtained in no-slip conditions.

5 Conclusion

With reference to a typical cross-section of the underground network in Catania (Italy) reported in Abate and Massimino (2016), the present paper deals with a FEM parametric analysis of the seismic response of the above-mentioned cross-section. This section involves a full-coupled tunnel–soil–aboveground building system. The depth of the tunnel, the position of the aboveground building with respect to the tunnel and seismic inputs were varied. Two tunnel depths, two building positions and thirty recorded accelerograms were adopted.

The results are presented in terms of acceleration amplification ratios, Fourier amplitude spectra and amplification functions. Bending moments and axial forces in the tunnel due to seismic loading obtained by means of the FEM modelling are also presented and compared with those obtained using well-known analytical approaches (Wang 1993; Penzien 2000), which refer to the simpler tunnel–soil interaction (neglecting the aboveground building). The latter comparison allows us to detect the potential of the analytical approaches, as well as their possible weaknesses, in evaluating bending moments and axial forces in the tunnel.

The main conclusions can be summarised as follows.

- *Effect of the presence of the tunnel* De-amplification occurs along the tunnel, this in turn leads to lower R_a at the soil surface in respect to free-field conditions. Thus, the parametric analysis confirms that tunnels in urban areas have beneficial effects in terms of amplification phenomena, as shown in Abate and Massimino (2016).
- *Effect of the tunnel depth* The shallower the tunnel, the lower the acceleration at the soil surface. The average amplification ratios are $R_{a,av} = 1.05$ for $f_s/f_m \leq 0.4$ and $R_{a,av} = 1.55$ for $f_s/f_m > 0.4$ in the case of the shallow tunnel and $R_{a,av} = 1.30$ for $f_s/f_m \leq 0.4$ and $R_{a,av} = 1.88$ for $f_s/f_m > 0.4$ for the deep tunnel. Generally, de-amplification occurs across the tunnel. For some cases characterised by $f_s/f_m \leq 0.4$ de-amplification occurs at the soil surface. Amplification across the layer above the tunnel is stronger compared to the amplification from the bedrock to the tunnel. This is due to the softer soil profile approaching the soil surface.
- *Effect of the position of the aboveground building* The building represents a surcharge, which reduces amplification phenomena. The combined de-amplification effects due to the tunnel and the aboveground building are highest when the building is aligned to the tunnel.
- *Effect of frequency* The occurrence of $f_s/f_m > 0.4$ often leads to more severe responses in terms of R_a in comparison with those related to $f_s/f_m \leq 0.4$, being f_s the natural frequency of the whole system and f_m the average fundamental frequency of the input.
- *Predominant frequency* The filtering effect of the system in terms of predominant frequency is important and varies with the tunnel depth and building position.
- *Tunnel bending moments* Generally, it is possible to observe a quite good agreement between numerical and analytical results. In particular, when computing γ_{max} with the full-coupled FEM modelling the agreement between the numerical and analytical results is more remarkable. The nearer the building, the higher the dynamic bending moments. No clear effects are observed in terms of tunnel depth.
- *Tunnel axial forces* In terms of axial forces the difference between full-slip and no-slip conditions is evident. Analytical solutions for no-slip conditions are more conservative and close to the numerical results obtained in no-slip conditions.
- Analyses of the full-coupled tunnel–soil–aboveground building system appear necessary up to the maximum investigated tunnel depth (18 m) and the maximum investigated building distance (20 m). Other FEM analyses, increasing the building

distance and the tunnel depth, could be developed in the future to determine the limit values of the building distance and the tunnel depth from which the considerations on full-coupled systems are not necessary.

Appendix

This Appendix reports some additional results regarding the response of the whole system to the thirty inputs in terms of accelerations. More precisely, Figs. 14 and 15 show the influence of the tunnel depth and of the building position on the amplification ratio along the axis of the tunnel, respectively. Figure 16 reports the accelerations at points A; Fig. 17 reports the accelerations at points B and C. Figure 16 allows us to quantify the acceleration that hit the aboveground structure. Figure 17 allows us to quantify the frequent de-amplification through the tunnel.

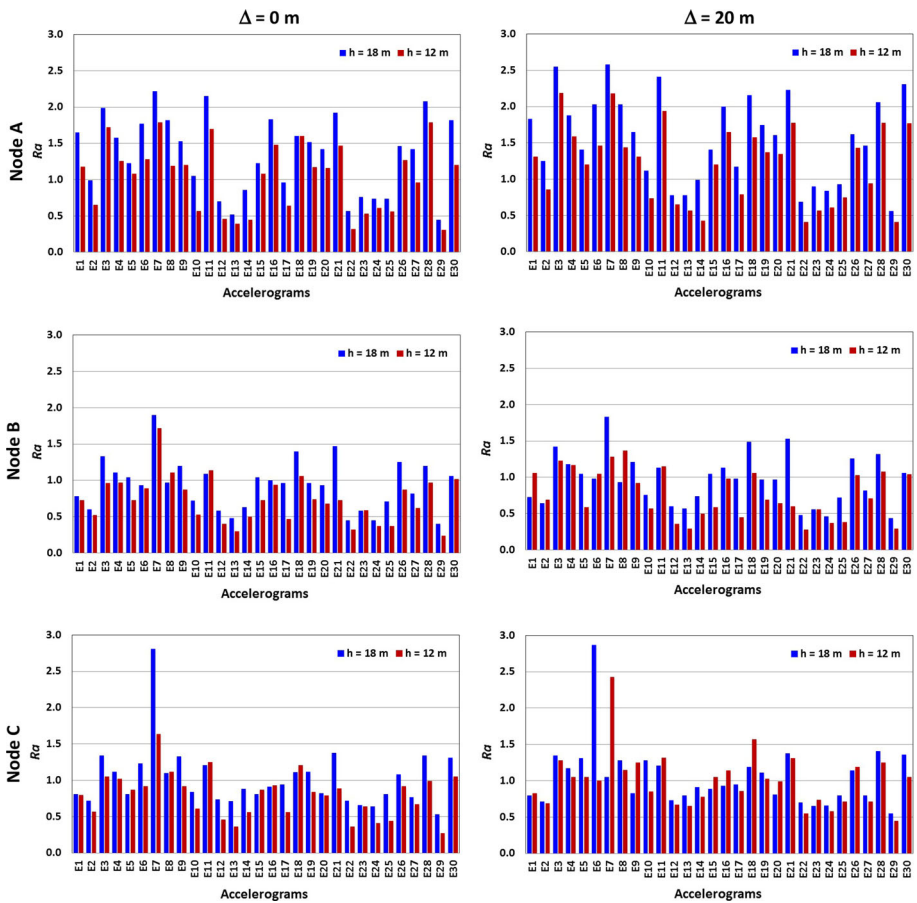


Fig. 14 Influence of the tunnel depth on the amplification ratio along the axis of the tunnel (A–B–C alignment)

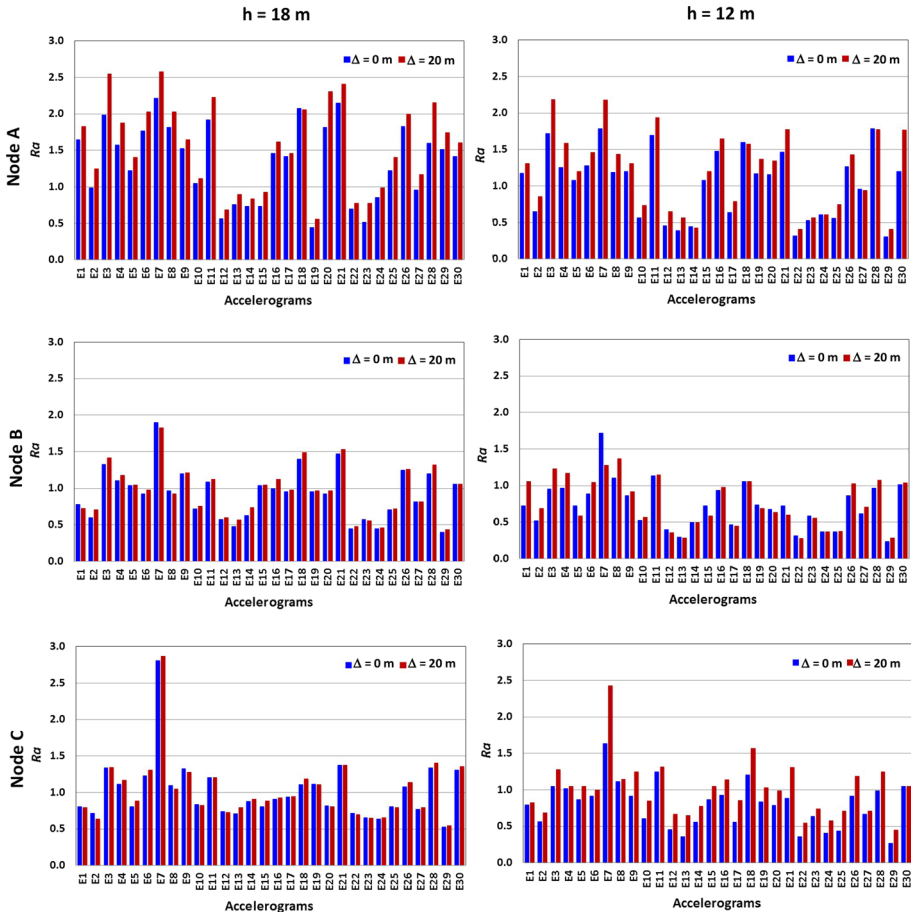


Fig. 15 Influence of the building position on the amplification ratio along the axis of the tunnel (A–B–C alignment)

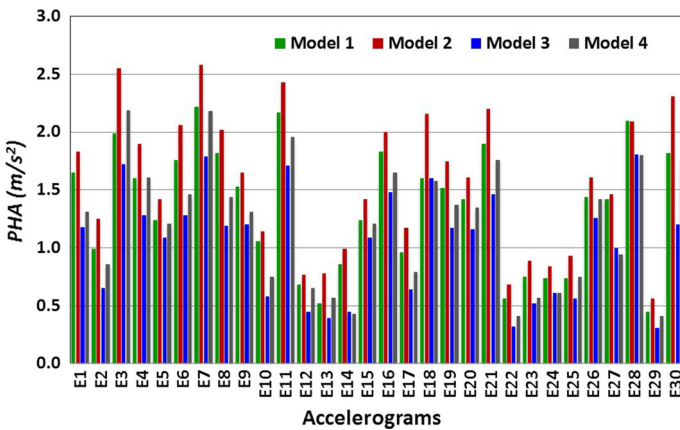


Fig. 16 Maxima horizontal accelerations at points A

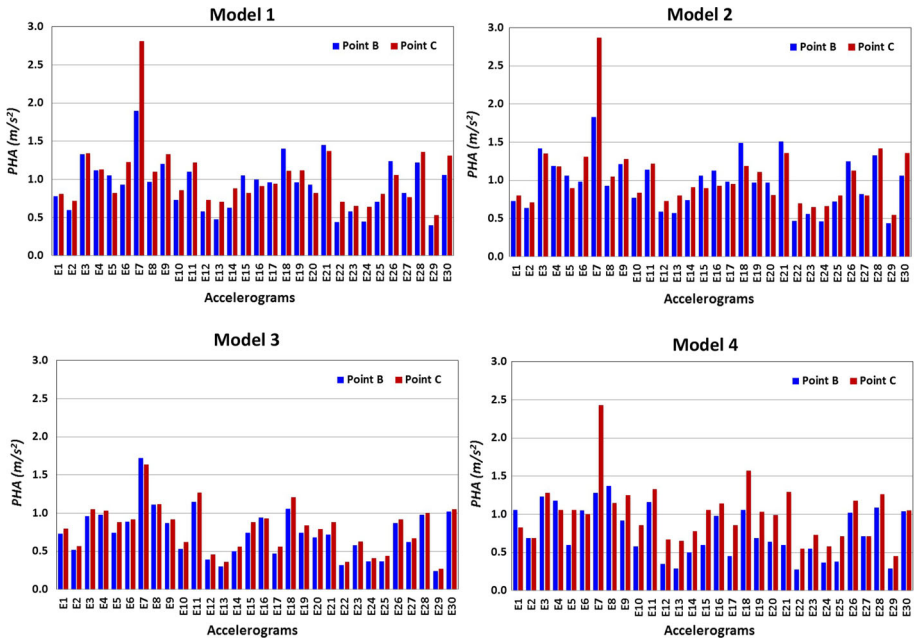


Fig. 17 Comparison between maxima horizontal accelerations at points B (*tunnel upper boundary*) and C (*tunnel lower boundary*)

References

- Abate G, Massimino MR (2016) Numerical modelling of the seismic response of a tunnel–soil–aboveground building system in Catania (Italy). *Bull Earthq Eng*. doi:10.1007/s10518-016-9973-9
- Abate G, Bosco M, Massimino MR, Maugeri M (2006) Limit state analysis for the Catania fire-station (Italy). In: 8th US national conference on earthquake engineering 2006, vol 11. pp 6532–6541
- Abate G, Massimino MR, Maugeri M (2008) Finite element modeling of a shaking table test to evaluate the dynamic behaviour of a soil–foundation system. In: AIP conference proceedings, vol 1020, issue PART 1, 2008. pp 569–576
- Abate G, Massimino MR, Maugeri M, Muir Wood D (2010) Numerical modelling of a shaking table test for soil–foundation–superstructure interaction by means of a soil constitutive model implemented in a FEM code. *Geotech Geol Eng* 28:37–59
- Abate G, Massimino MR, Maugeri M (2015) Numerical modelling of centrifuge tests on tunnel–soil systems. *Bull Earthq Eng* 13(7):1927–1951
- ADINA (2008) Automatic dynamic incremental nonlinear analysis: theory and modelling guide. ADINA R&D, Inc., Watertown
- AFPS/AFTES (2001) Guidelines on earthquake design and protection of underground structures. Working group of the French association for seismic engineering (AFPS) and French Tunnelling Association (AFTES) Version 1
- Anastasopoulos I, Gazetas G (2010) Analysis of cut-and-cover tunnels against large tectonic deformation. *Bull Earthq Eng* 8:283–307
- Anastasopoulos I, Gerolymos N, Drosos V, Kourkoulis R, Georgarakos T, Gazetas G (2007) Nonlinear response of deep immersed tunnel to strong seismic shaking. *J Geotech Geoenviron Eng* 133(9):1067–1090
- Anastasopoulos I, Gerolymos N, Drosos V, Georgarakos T, Kourkoulis R, Gazetas G (2008) Behaviour of deep immersed tunnel under combined normal fault rupture deformation and subsequent seismic shaking. *Bull Earthq Eng* 6:213–239

- Bardet JB, Ichii K, Lin CH (2000) EERA: a computer program for equivalent-linear earthquake site response analyses of layered soil deposits. University of Southern California, Department of Civil Engineering, Los Angeles
- Bathe KJ (1996) Finite element procedures. Prentice Hall, Englewood Cliffs
- Chang DW, Roesset JM, Wen CH (2000) A time-domain viscous damping model based on frequency-dependent damping ratios. *Soil Dyn Earthq Eng* 19:551–558
- De Barros FCP, Luco JE (1993) Diffraction of obliquely incident waves by a cylindrical cavity embedded in a layered viscoelastic halfspace. *Soil Dyn Earthq Eng* 12:159–171
- EC8 (2003) Design of structures for earthquake resistance. European Pre-standard. ENV 1998. European Com. for Standard. Bruxelles
- FHWA (2009) Technical manual for design and construction of road tunnels—Civil elements, U.S. Department of transportation, Federal Highway Administration, Publication No. FHWA-NHI-09-010, March 2009
- Gajo A, Muir Wood D (1997) Numerical analysis of behaviour of shear stacks under dynamic loading. Report of ECOEST Project, EERC Laboratory, Bristol University
- Gazetas G (2014) Case histories of tunnel failures during earthquakes and during construction. In: Proceedings of the half-day conference, a tunnel/underground station failure conference, by the Israeli Geotechnical Society, 19 Jan, 2014
- Grassi F, Massimino MR (2009) Evaluation of kinematic bending moments in a pile foundation using the finite element approach. *WIT Trans Built Environ* 104(2009):479–488
- Hashash YMA, Hook JJ, Schmidt B, Yao JIC (2001) Seismic design and analysis of underground structures. *Tunn Undergr Space Technol* 16:247–293
- Hashash YMA, Park D, Yao JIC (2005) Ovaling deformations of circular tunnels under seismic loading, an update on seismic design and analysis of underground structures. *Tunn Undergr Space Technol* 20(2005):435–441
- Huo H, Bodet A, Fernández G, Ramírez J (2005) Load transfer mechanisms between underground structure and surrounding ground: evaluation of the failure of the Daikai station. *J Geotech Geoenviron Eng* 131(12):1522–1533
- Idriss IM, Seed HB (1968) Seismic response of horizontal soil layers. *J Soil Mech Found Div ASCE* 94(SM4):1003–1031
- Kawashima K (2000) Seismic design of underground structures in soft ground: a review. In: Fujita, Miyazaki (eds) Geotechnical aspects of underground construction in soft ground. Balkema, Rotterdam
- Kirtas E, Rovithis E, Ptilakis K (2009) Subsoil Interventions Effect on Structural Seismic Response. Part I: Validation of Numerical Simulations. *J Earthq Eng* 13:155–169
- Kontoe S, Zdravkovic L, Potts D, Mentiki C (2008) Case study on seismic tunnel response. *Can Geotech J* 45:1743–1764
- Kouretzis G, Bouckovalas G, Sofianos A, YioutaMitra P (2007) Detrimental effects of urban tunnels on design seismic ground motions. In: Proceedings of the 2nd Japan-Greece workshop on seismic design, observation, and retrofit of foundations, April 3–4, 2007, Tokyo, Japan
- Lanzano G, Bilotta E, Russo G, Silvestri F, Madabhushi SPG (2012) Centrifuge modelling of seismic loading on tunnels in sand. *Geotech Test J* 35(6):854–869. doi:[10.1520/GTJ104348](https://doi.org/10.1520/GTJ104348)
- Lanzo G, Pagliaroli A, D'Elia B (2003) Numerical study on the frequency-dependent viscous damping in dynamic response analyses of ground. In: Proceedings on earthquake resistant engineering structures IV conference. pp 315–324. doi: [10.2495/ER030301](https://doi.org/10.2495/ER030301)
- Lee VW, Karl J (1992) Diffraction of SV-waves by underground, circular, cylindrical cavities. *Soil Dyn Earthq Eng* 11:445–456
- Luco JE, De Barros FCP (1994) Dynamic Displacements and stresses in the vicinity of a cylindrical cavity embedded in a half-space. *Earthq Eng Struct Dyn* 23:321–340
- Maugeri M, Abate G, Massimino MR (2012) Soil-structure interaction for seismic improvement of noto cathedral (Italy). *Geotech Geol Earthq Eng* 16:217–239
- Merritt JL, Monsee JE, Hendron AJ Jr (1985) Seismic design of underground structures. In: Proceedings of the 1985 rapid excavation tunneling conference, vol 1. pp 104–131
- NTC (2008) D.M. 14/01/08—Norme tecniche per le costruzioni, Gazzetta Ufficiale Repubblica Italiana, 14-01-08 (in Italian)
- Penzien J (2000) Seismically induced racking of tunnel linings. *Earthq Eng Struct Dyn* 29:684–691
- Ptilakis K, Tsinidis G (2014) Performance and seismic design of underground structures. In: Maugeri M, Soccodato C (eds) Earthquake geotechnical engineering design. Geotechnical, geological and earthquake engineering, vol 28. Springer International Publishing, Switzerland, pp 279–340. doi:[10.1007/978-3-319-03182-8_11](https://doi.org/10.1007/978-3-319-03182-8_11)

- Pitilakis K, Tsinidis G, Leanza A, Maugeri M (2014) Seismic behaviour of circular tunnels accounting for above ground structures interaction effects. *Soil Dyn Earthq Eng* 67:1–15
- Power M, Rosidi D, Kaneshiro J, Gilstrap S, Chiou SJ (1998) Summary and evaluation of procedures for the seismic design of tunnels. Final Report for Task 112-d-5.3(c). National Center for Earthquake Engineering Research, Buffalo, New York
- Rathje EM, Abrahamson NA, Bray JD (1998) Simplified frequency content estimates of earthquake ground motions. *J Geotech Geoenviron Eng ASCE* 124(2):150–158
- Sedarat H, Kozak A, Hashash YMA, Shamsabadi A, Krimotat A (2009) Contact interface in seismic analysis of circular tunnels. *Tunnel Undergr Space Technol* 24(4):482–490
- Smerzini C, Aviles J, Paolucci R, Sanchez-Sesma FJ (2009) Effect of underground cavities on surface earthquake ground motion under SH wave propagation. *Earthq Eng Struct Dynam* 38:1441–1460
- St. John CM, Zahrah TF (1987) Aseismic design of underground structures. *Tunnel Undergr Space Technol* 2(2):165–197
- Tsinidis G, Pitilakis K, Trikalioti AD (2013a) Numerical simulation of round robin numerical test on tunnels using a simplified kinematic hardening Model. *Acta Geotech*. doi:[10.1007/s11440-013-0293-9](https://doi.org/10.1007/s11440-013-0293-9)
- Tsinidis G, Pitilakis K, Heron C, Madabhushi G (2013b) Experimental and numerical investigation of the seismic behaviour of rectangular tunnels in soft soils. In: Papadrakakis M, Papadopoulos V, Plevris V (eds) *COMPDYN 2013, 4th ECCOMAS thematic conference on computational methods in structural dynamics and earthquake engineering*, Kos Island, Greece, 12–14 June 2013
- Wang JN (1993) *Seismic design of tunnels: a simple state of the art design approach*. Parsons Brinckerhoff Inc., New York
- Wang WL, Wang TT, Su JJ, Lin CH, Sengineering CR, Huang TH (2001) Assessment of damage in mountain tunnels due to the Taiwan Chi-Chi earthquake. *Tunnel Undergr Space Technol* 16:133–150
- Wang ZZ, Gao B, Jiang YJ, Yuan S (2009) Investigation and assessment on mountain tunnels and geotechnical damage after the Wenchuan earthquake. *Sci China Ser E Technol Sci* 52(2):549–558
- Wang HF, Lou ML, Chen X, Zhai YM (2013) Structure–soil–structure interaction between underground structure and ground structure. *Soil Dyn Earthq Eng* 54:31–38